Source Breakup Dynamics in Au + Au Collisions at $\sqrt{s_{NN}} = 200$ GeV via Three-Dimensional Two-Pion Source Imaging

S. Afanasiev,[17] C. Aidala,[7] N. N. Ajitanand,[43] Y. Akiba,[37,38] J. Alexander,[43] A. Al-Jamel,[33] K. Aoki,[23,37] L. Aphecetche,[45] R. Armendariz,[33] S. H. Aronson,[3] R. Averbeck,[44] T. C. Awes,[34] B. Azmoun,[3] V. Babintsev,[14] A. Baldisseri,[8] K. N. Barish,[4] P. D. Barnes,[26] B. Bassalleck,[32] S. Bathe,[4] S. Batsouli,[7] V. Baublis,[36] F. Bauer,[4] A. Bazilevsky,[3] S. Belikov,[3,16,*] R. Bennett,[44] Y. Berdnikov,[40] M. T. Bjorndal,[7] J. G. Boissevain,[26] H. Borel,[8] K. Boyle,[44] M. L. Brooks,[26] D. S. Brown,[33] D. Bucher,[29] H. Buesching,[3] V. Bumazhnov,[14] G. Bunce,[3,38] J. M. Burward-Hoy,[26] S. Butsyk,[44] S. Campbell,[44] J.-S. Chai,[18] S. Chernichenko,[14] J. Chiba,[19] C. Y. Chi,[7] M. Chiu,[7] I. J. Choi,[52] T. Chujo,[49] P. Chung,[43] V. Cianciolo,[34] C. R. Cleven,[12] Y. Cobigo,[8] B. A. Cole,[7] M. P. Comets,[35] P. Constantin,[16] M. Csanád,[10] T. Csörgő,[20] T. Dahms,[44] K. Das,[11] G. David,[3] H. Delagrange,[45] A. Denisov,[14] D. d'Enterria,[7] A. Deshpande,[38,44] E. J. Desmond,[3] O. Dietzsch,[41] A. Dion,[44] J. L. Drachenberg,[1] O. Drapier,[24] A. Drees,[44] A. K. Dubey,[51] A. Durum,[14] V. Dzhordzhadze,[46] Y. V. Efremenko,[34] J. Egdemir,[44] A. Enokizono,[13] H. En'yo,[37,38] B. Espagnon,[35] S. Esumi,[48] D. E. Fields,[32,38] F. Fleuret,[24] S. L. Fokin,[22] B. Forestier,[27] Z. Fraenkel,[51,*] J. E. Frantz,[7] A. Franz,[3] A. D. Frawley,[11] Y. Fukao,[23,37] S.-Y. Fung,[4] S. Gadrat,[27] F. Gastineau,[45] M. Germain,[45] A. Glenn,[46] M. Gonin,[24] J. Gosset,[8] Y. Goto,[37,38] R. Granier de Cassagnac,[24] N. Grau,[16] S. V. Greene,[49] M. Grosse Perdekamp,[15,38] T. Gunji,[5] H.-Å. Gustafsson,[28] T. Hachiya,[13,37] A. Hadj Henni,[45] J. S. Haggerty,[3] M. N. Hagiwara,[1] H. Hamagaki,[5] H. Harada,[13] E. P. Hartouni,[25] K. Haruna,[13] M. Harvey,[3] E. Haslum,[28] K. Hasuko,[37] R. Hayano,[5] M. Heffner,[25] T. K. Hemmick,[44] J. M. Heuser,[37] X. He,[12] H. Hiejima,[15] J. C. Hill,[16] R. Hobbs,[32] M. Holmes,[49] W. Holzmann,[43] K. Homma,[13] B. Hong,[21] T. Horaguchi,[37,47] M. G. Hur,[18] T. Ichihara,[37,38] K. Imai,[23,37] M. Inaba,[48] D. Isenhower,[1] L. Isenhower,[1] M. Ishihara,[37] T. Isobe,[5] M. Issah,[43] A. Isupov,[17] B. V. Jacak,[44,†] J. Jia,[7] J. Jin,[7] O. Jinnouchi,[38] B. M. Johnson,[3] K. S. Joo,[30] D. Jouan,[35] F. Kajihara,[5,37] S. Kametani,[5,50] N. Kamihara,[37,47] M. Kaneta,[38] J. H. Kang,[52] T. Kawagishi,[48] A. V. Kazantsev,[22] S. Kelly,[6] A. Khanzadeev,[36] D. J. Kim,[52] E. Kim,[42] Y.-S. Kim,[18] E. Kinney,[6] A. Kiss,[10] E. Kistenev,[3] A. Kiyomichi,[37] C. Klein-Boesing,[29] L. Kochenda,[36] V. Kochetkov,[14] B. Komkov,[36] M. Konno,[48] D. Kotchetkov,[4] A. Kozlov,[51] P. J. Kroon,[3] G. J. Kunde,[26] N. Kurihara,[5] K. Kurita,[39,37] M. J. Kweon,[21] Y. Kwon,[52] G. S. Kyle,[33] R. Lacey,[43] J. G. Lajoie,[16] A. Lebedev,[16] Y. Le Bornec,[35] S. Leckey,[44] D. M. Lee,[26] M. K. Lee,[52] M. J. Leitch,[26] M. A. L. Leite,[41] H. Lim,[42] A. Litvinenko,[17] M. X. Liu,[26] X. H. Li,[4] C. F. Maguire,[49] Y. I. Makdisi,[3] A. Malakhov,[17] M. D. Malik,[32] V. I. Manko,[22] H. Masui,[48] F. Matathias,[44] M. C. McCain,[15] P. L. McGaughey,[26] Y. Miake,[48] T. E. Miller,[49] A. Milov,[44] S. Mioduszewski,[3] G. C. Mishra,[12] J. T. Mitchell,[3] D. P. Morrison,[3] J. M. Moss,[26] T. V. Moukhanova,[22] D. Mukhopadhyay,[49] J. Murata,[39,37] S. Nagamiya,[19] Y. Nagata,[48] J. L. Nagle,[6] M. Naglis,[51] T. Nakamura,[13] J. Newby,[25] M. Nguyen,[44] B. E. Norman,[26] A. S. Nyanin,[22] J. Nystrand,[28] E. O'Brien,[3] C. A. Ogilvie,[16] H. Ohnishi,[37] I. D. Ojha,[49] H. Okada,[23,37] K. Okada,[38] O. O. Omiwade,[1] A. Oskarsson,[28] I. Otterlund,[28] K. Ozawa,[5] D. Pal,[49] A. P. T. Palounek,[26] V. Pantuev,[44] V. Papavassiliou,[33] J. Park,[42] W. J. Park,[21] S. F. Pate,[33] H. Pei,[16] J.-C. Peng,[15] H. Pereira,[8] V. Peresedov,[17] D. Yu. Peressounko,[22] C. Pinkenburg,[3] R. P. Pisani,[3] M. L. Purschke,[3] A. K. Purwar,[44] H. Qu,[12] J. Rak,[16] I. Ravinovich,[51] K. F. Read,[34,46] M. Reuter,[44] K. Reygers,[29] V. Riabov,[36] Y. Riabov,[36] G. Roche,[27] A. Romana,[24,*] M. Rosati,[16] S. S. E. Rosendahl,[28] P. Rosnet,[27] P. Rukoyatkin,[17] V. L. Rykov,[37] S. S. Ryu,[52] B. Sahlmueller,[29] N. Saito,[23,37,38] T. Sakaguchi,[5,50] S. Sakai,[48] V. Samsonov,[36] H. D. Sato,[23,37] S. Sato,[3,19,48] S. Sawada,[19] V. Semenov,[14] R. Seto,[4] D. Sharma,[51] T. K. Shea,[3] I. Shein,[14] T.-A. Shibata,[37,47] K. Shigaki,[13] M. Shimomura,[48] T. Shohjoh,[48] K. Shoji,[23,37] A. Sickles,[44] C. L. Silva,[41] D. Silvermyr,[34] K. S. Sim,[21] C. P. Singh,[2] V. Singh,[2] S. Skutnik,[16] W. C. Smith,[1] A. Soldatov,[14] R. A. Soltz,[25] W. E. Sondheim,[26] S. P. Sorensen,[46] I. V. Sourikova,[3] F. Staley,[8] P. W. Stankus,[34] E. Stenlund,[28] M. Stepanov,[33] A. Ster,[20] S. P. Stoll,[3] T. Sugitate,[13] C. Suire,[35] J. P. Sullivan,[26] J. Sziklai,[20] T. Tabaru,[38] S. Takagi,[48] E. M. Takagui,[41] A. Taketani,[37,38] K. H. Tanaka,[19] Y. Tanaka,[31] K. Tanida,[37,38] M. J. Tannenbaum,[3] A. Taranenko,[43] P. Tarján,[9] T. L. Thomas,[32] M. Togawa,[23,37] J. Tojo,[37] H. Torii,[37] R. S. Towell,[1] V-N. Tram,[24] I. Tserruya,[51] Y. Tsuchimoto,[13,37] S. K. Tuli,[2] H. Tydesjö,[28] N. Tyurin,[14] C. Vale,[16] H. Valle,[49] H. W. van Hecke,[26] J. Velkovska,[49] R. Vertesi,[9] A. A. Vinogradov,[22] E. Vznuzdaev,[36] M. Wagner,[23,37] X. R. Wang,[33] Y. Watanabe,[37,38] J. Wessels,[29] S. N. White,[3] N. Willis,[35] D. Winter,[7] C. L. Woody,[3] M. Wysocki,[6] W. Xie,[4,38] A. Yanovich,[14] S. Yokkaichi,[37,38] G. R. Young,[34] I. Younus,[32] I. E. Yushmanov,[22] W. A. Zajc,[7] O. Zaudtke,[29] C. Zhang,[7] J. Zimányi,[20,*] and L. Zolin[17]

(PHENIX Collaboration)

[1]*Abilene Christian University, Abilene, Texas 79699, USA*
[2]*Department of Physics, Banaras Hindu University, Varanasi 221005, India*

[3]Brookhaven National Laboratory, Upton, New York 11973-5000, USA
[4]University of California–Riverside, Riverside, California 92521, USA
[5]Center for Nuclear Study, Graduate School of Science, University of Tokyo, 7-3-1 Hongo, Bunkyo, Tokyo 113-0033, Japan
[6]University of Colorado, Boulder, Colorado 80309, USA
[7]Columbia University, New York, New York 10027, USA and Nevis Laboratories, Irvington, New York 10533, USA
[8]Dapnia, CEA Saclay, F-91191, Gif-sur-Yvette, France
[9]Debrecen University, H-4010 Debrecen, Egyetem tér 1, Hungary
[10]ELTE, Eötvös Loránd University, H - 1117 Budapest, Pázmány P. s. 1/A, Hungary
[11]Florida State University, Tallahassee, Florida 32306, USA
[12]Georgia State University, Atlanta, Georgia 30303, USA
[13]Hiroshima University, Kagamiyama, Higashi-Hiroshima 739-8526, Japan
[14]IHEP Protvino, State Research Center of Russian Federation, Institute for High Energy Physics, Protvino, 142281, Russia
[15]University of Illinois at Urbana-Champaign, Urbana, Illinois 61801, USA
[16]Iowa State University, Ames, Iowa 50011, USA
[17]Joint Institute for Nuclear Research, 141980 Dubna, Moscow Region, Russia
[18]KAERI, Cyclotron Application Laboratory, Seoul, Korea
[19]KEK, High Energy Accelerator Research Organization, Tsukuba, Ibaraki 305-0801, Japan
[20]KFKI Research Institute for Particle and Nuclear Physics of the Hungarian Academy of Sciences (MTA KFKI RMKI), H-1525 Budapest 114, PO Box 49, Budapest, Hungary
[21]Korea University, Seoul, 136-701, Korea
[22]Russian Research Center "Kurchatov Institute," Moscow, Russia
[23]Kyoto University, Kyoto 606-8502, Japan
[24]Laboratoire Leprince-Ringuet, Ecole Polytechnique, CNRS-IN2P3, Route de Saclay, F-91128, Palaiseau, France
[25]Lawrence Livermore National Laboratory, Livermore, California 94550, USA
[26]Los Alamos National Laboratory, Los Alamos, New Mexico 87545, USA
[27]LPC, Université Blaise Pascal, CNRS-IN2P3, Clermont-Fd, 63177 Aubiere Cedex, France
[28]Department of Physics, Lund University, Box 118, SE-221 00 Lund, Sweden
[29]Institut für Kernphysik, University of Muenster, D-48149 Muenster, Germany
[30]Myongji University, Yongin, Kyonggido 449-728, Korea
[31]Nagasaki Institute of Applied Science, Nagasaki-shi, Nagasaki 851-0193, Japan
[32]University of New Mexico, Albuquerque, New Mexico 87131, USA
[33]New Mexico State University, Las Cruces, New Mexico 88003, USA
[34]Oak Ridge National Laboratory, Oak Ridge, Tennessee 37831, USA
[35]IPN-Orsay, Universite Paris Sud, CNRS-IN2P3, BP1, F-91406, Orsay, France
[36]PNPI, Petersburg Nuclear Physics Institute, Gatchina, Leningrad region, 188300, Russia
[37]RIKEN, The Institute of Physical and Chemical Research, Wako, Saitama 351-0198, Japan
[38]RIKEN BNL Research Center, Brookhaven National Laboratory, Upton, New York 11973-5000, USA
[39]Physics Department, Rikkyo University, 3-34-1 Nishi-Ikebukuro, Toshima, Tokyo 171-8501, Japan
[40]Saint Petersburg State Polytechnic University, St. Petersburg, Russia
[41]Universidade de São Paulo, Instituto de Física, Caixa Postal 66318, São Paulo CEP05315-970, Brazil
[42]System Electronics Laboratory, Seoul National University, Seoul, Korea
[43]Chemistry Department, Stony Brook University, SUNY, Stony Brook, New York 11794-3400, USA
[44]Department of Physics and Astronomy, Stony Brook University, SUNY, Stony Brook, New York 11794, USA
[45]SUBATECH (Ecole des Mines de Nantes, CNRS-IN2P3, Université de Nantes) BP 20722 - 44307, Nantes, France
[46]University of Tennessee, Knoxville, Tennessee 37996, USA
[47]Department of Physics, Tokyo Institute of Technology, Oh-okayama, Meguro, Tokyo 152-8551, Japan
[48]Institute of Physics, University of Tsukuba, Tsukuba, Ibaraki 305, Japan
[49]Vanderbilt University, Nashville, Tennessee 37235, USA
[50]Waseda University, Advanced Research Institute for Science and Engineering, 17 Kikui-cho, Shinjuku-ku, Tokyo 162-0044, Japan
[51]Weizmann Institute, Rehovot 76100, Israel
[52]Yonsei University, IPAP, Seoul 120-749, Korea

(Received 28 December 2007; published 13 June 2008)

A three-dimensional correlation function obtained from midrapidity, low p_T, pion pairs in central Au + Au collisions at $\sqrt{s_{NN}} = 200$ GeV is studied. The extracted model-independent source function indicates a long range tail in the directions of the pion pair transverse momentum (out) and the beam (long). A proper breakup time $\tau_0 \sim 9$ fm/c and a mean proper emission duration $\Delta\tau \sim 2$ fm/c, leading to sizable emission time differences ($\langle|\Delta t_{\mathrm{LCM}}|\rangle \approx 12$ fm/c), are required to allow models to be successfully matched to these tails. The model comparisons also suggest an outside-in "burning" of the emission source reminiscent of many hydrodynamical models.

DOI: 10.1103/PhysRevLett.100.232301 PACS numbers: 25.75.Ld

Collisions between heavy nuclei at ultrarelativistic energies produce transient systems with energy densities much greater than that required to decompose bulk nuclear matter into quarks and gluons [1]. Such systems were predicted to have long lifetimes if a first order phase transition occurred during their formation or decay [2].

A number of interferometry studies [3] have been made to search for signals of long time delays in emissions from actual reaction sources [4]. For a Gaussian source function, assumed in the traditional Hanbury Brown–Twiss methodology, this would be signaled by an increase in the width R of the emission source function in the out direction of the Berstch-Pratt coordinate system, i.e., $R_{\rm out}/R_{\rm side} \gg 1$. In this system, ''out'' designates the direction of the pair total transverse momentum, ''long'' designates the beam direction, and ''side'' is perpendicular to ''long'' and ''out.'' No such result has been found by these Hanbury Brown–Twiss studies and the reported Gaussian source functions are spheroidal with $R_{\rm out} \approx R_{\rm side}$ in the longitudinally comoving system (LCMS) [4]. However, a recent study with a one-dimensional (1D) source imaging technique [5] has observed a long non-Gaussian tail in the radial source function and attributed it to possible lifetime effects [6,7]. This suggests that further study of the source image may give new insights into the reaction dynamics leading to source breakup.

Here, we extract and perform a detailed study of the 3D two-pion source function using the technique proposed by Danielewicz and Pratt [8,9]. Namely, the 3D correlation function is first decomposed into a basis of Cartesian surface-spherical harmonics to extract the coefficients, also called moments, of the expansion. In turn, they are then imaged or fitted with a trial function to extract the 3D source function, which is then used to probe the emission dynamics of the pion source produced.

Au + Au data (at $\sqrt{s_{NN}} = 200$ GeV) were recorded during 2004 with the PHENIX detector [10] at the Relativistic Heavy Ion Collider (RHIC). The collision vertex z (along the beam axis) was constrained to $|z| < 30$ cm of the nominal crossing point. Charged pions were detected in the east and west central arms of PHENIX, each of which subtends 90° in azimuth ϕ, and ± 0.35 units of pseudorapidity η. Tracking and momentum reconstruction were accomplished with the drift chamber and two layers of multiwire proportional chambers with pad readout (PC1 and PC3). Particle momenta were measured with a resolution $\sigma_p/p = 0.7\% \oplus 1.0\% p$ (GeV/c).

Pion identification was achieved for transverse momentum $p_t \lesssim 2.0$ GeV/c and $p_t \lesssim 1$ GeV/c in the time of flight and electromagnetic calorimeter, respectively. For this analysis, midrapidity ($-0.35 < y < 0.35$, where y is particle rapidity in the nucleus-nucleus center of mass frame) pion pairs were selected with $0.2 < p_T < 0.36$ GeV/c, where p_T is half the pion pair total transverse momentum, from semicentral (0%–20%) Au + Au collisions at $\sqrt{s_{NN}} = 200$ GeV. Track merging and splitting effects were removed by appropriate cuts on both the real and mixed pair distributions [7]. Systematic variations of these cuts were explored to obtain systematic error estimates; on average, they are well within the statistical uncertainty. Hence, the pair cuts do not introduce any significant bias in the correlation function.

The 3D correlation function $C(\mathbf{q}) = N_{\rm fgd}(\mathbf{q})/N_{\rm bkg}(\mathbf{q})$ was constructed as a ratio of 3D relative momentum distribution for $\pi^+\pi^+$ and $\pi^-\pi^-$ pairs in the same event $N_{\rm fgd}(\mathbf{q})$ to that from mixed events $N_{\rm bkg}(\mathbf{q})$. Here, $\mathbf{q} = \frac{(\mathbf{p}_1 - \mathbf{p}_2)}{2}$ where $\mathbf{p}_1$ and $\mathbf{p}_2$ are the momentum 4-vectors in the pair center of mass system (PCMS). The Lorentz transformation of $\mathbf{q}$ from the laboratory frame to the PCMS is made by first transforming to the pair LCMS along the beam direction and then to the PCMS along the pair transverse momentum [11]. $C(\mathbf{q})$ is flat and normalized to unity over $50 < |\mathbf{q}| < 100$ MeV/c.

To obtain the moments, the 3D correlation function $C(\mathbf{q})$ is expanded in a Cartesian harmonic basis [8,9]

$$C(\mathbf{q}) - 1 = R(\mathbf{q}) = \sum_{l,\alpha_1,\ldots,\alpha_l} R^l_{\alpha_1,\ldots,\alpha_l}(q) A^l_{\alpha_1,\ldots,\alpha_l}(\Omega_{\mathbf{q}}) \quad (1)$$

where $l = 0, 1, 2, \ldots$, $\alpha_i = x$, y or z, $A^l_{\alpha_1,\ldots,\alpha_l}(\Omega_{\mathbf{q}})$ are Cartesian harmonic basis elements ($\Omega_{\mathbf{q}}$ is the solid angle in $\mathbf{q}$ space), $R^l_{\alpha_1,\ldots,\alpha_l}(q)$ are Cartesian correlation moments given by Eq. (2), and q is the modulus of $\mathbf{q}$.

$$R^l_{\alpha_1,\ldots,\alpha_l}(q) = \frac{(2l+1)!!}{l!} \int \frac{d\Omega_{\mathbf{q}}}{4\pi} A^l_{\alpha_1,\ldots,\alpha_l}(\Omega_{\mathbf{q}}) R(\mathbf{q}). \quad (2)$$

Here, the coordinate axes are oriented so that z (long) is parallel to the beam direction and x (out) points in the direction of the total transverse momentum of the pair.

Correlation moments can be calculated from the measured 3D correlation function using Eq. (2). In this analysis, Eq. (1) is truncated at $l = 6$ and expressed in terms of independent moments only. As expected from symmetry considerations, odd moments were consistent with zero within statistical uncertainty; higher order moments were negligible [12]. Up to order 6, there are 10 independent moments: R^0, R^2_{x2}, R^2_{y2}, R^4_{x4}, R^4_{y4}, R^4_{x2y2}, R^6_{x6}, R^6_{y6}, R^6_{x4y2}, and R^6_{x2y4} (R^2_{x2} is shorthand for R^2_{xx}, dependent moments are obtained from independent ones [8,9]). These independent moments were extracted as a function of q by fitting the truncated series to the measured 3D correlation function with the moments as the parameters of the fit. The statistical error on the moments reflects the statistical error on the 3D correlation function.

Figure 1 shows the correlation moments $R^l_{\alpha_1,\ldots,\alpha_l}$ up to order $l = 6$. In 1(a), $R^0(q)$ is shown along with $R(q) = C(q) - 1$; both represent angle-averaged correlation functions, but $R^0(q)$ is obtained from the 3D correlation func-

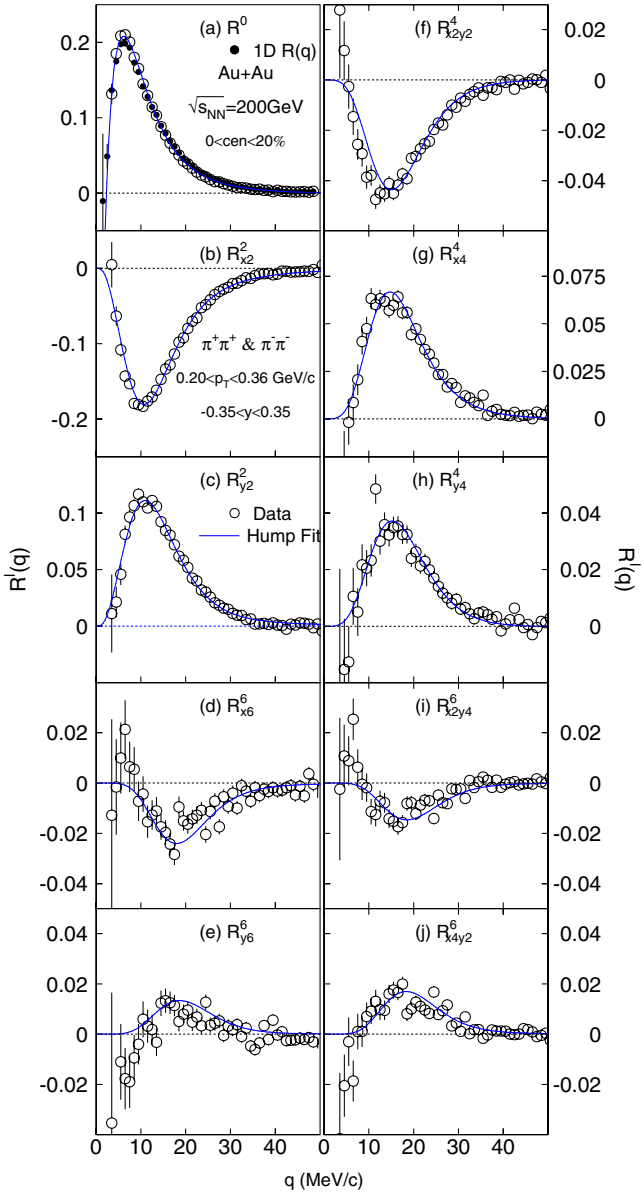

FIG. 1 (color online). Experimental correlation moments $R^l(q)$ for $l = 0, 2, 4, 6$. Panel (a) also shows a comparison between $R^0(q)$ and $R(q)$. Systematic errors are less than the statistical errors. The solid curves indicate the Hump function [Eq. (6)] fit.

tion via Eq. (1) while $R(q)$ is evaluated directly from the 1D correlation function as in Ref. [7].

The very good agreement between $R^0(q)$ and $R(q)$ underlines the absence of any significant angular acceptance issues and attests to the reliability of the moment extraction technique. Figures 1(b)–1(j) show that contributions decrease with increasing l in each direction and are relatively small for $l = 6$ [12]. This justifies truncating Eq. (1) at $l = 6$. The 3D source function $S(\mathbf{r})$ is obtained from these moments via imaging or fitting (see below).

Analogous to Eq. (1), $S(\mathbf{r})$ can be expanded in a Cartesian Surface-spherical harmonic basis [Eq. (3)]

$$S(\mathbf{r}) = \sum_l \sum_{\alpha_1,\ldots,\alpha_l} S^l_{\alpha_1,\ldots,\alpha_l}(r) A^l_{\alpha_1,\ldots,\alpha_l}(\Omega_{\mathbf{r}}). \tag{3}$$

Substitution of the series for $R(\mathbf{q})$ and $S(\mathbf{r})$ into the 3D Koonin-Pratt formalism [Eq. (4)] [3] gives a set of 1D relations [Eq. (5)] [8,9] which connects the correlation moments $R^l_{\alpha_1,\ldots,\alpha_l}(q)$ and source moments $S^l_{\alpha_1,\ldots,\alpha_l}(r)$.

$$C(\mathbf{q}) - 1 = R(\mathbf{q}) = \int d\mathbf{r} K(\mathbf{q}, \mathbf{r}) S(\mathbf{r}) \tag{4}$$

$$R^l_{\alpha_1,\ldots,\alpha_l}(q) = 4\pi \int dr r^2 K_l(q, r) S^l_{\alpha_1,\ldots,\alpha_l}(r). \tag{5}$$

$S(\mathbf{r})$ gives the probability of emitting a pair of particles with a separation vector $\mathbf{r}$ in the PCMS. The 3D kernel, $K(\mathbf{q}, \mathbf{r})$, incorporates Coulomb force and Bose-Einstein symmetrization. Strong interaction is assumed to be negligible for pions. Hence, no correction to the measured correlation function for Coulomb and other final-state interaction effects is required. The 1D imaging code of Brown and Danielewicz [5] was used to numerically invert each correlation moment $R^l_{\alpha_1,\ldots,\alpha_l}(q)$ to extract the corresponding source moment $S^l_{\alpha_1,\ldots,\alpha_l}(r)$; combining the latter as in Eq. (3) yielded the source function.

The 3D source function can also be extracted by directly fitting the 3D correlation function with an assumed functional form for $S(\mathbf{r})$. This corresponds to a simultaneous fit of the ten independent moments. A 4-parameter 3D Gaussian (ellipsoid) fit, using MINUIT minimization, gives a poor result ($\chi^2/\mathrm{ndf} = 3.7$, where ndf is the number of degrees of freedom). The solid curve in Fig. 1 shows the result of a fit to the independent moments with an empirical Hump function given by

$$S^H(r_x, r_y, r_z) = \lambda \exp\Big[-f_s\Big(\frac{x^2}{4r^2_{xs}} + \frac{y^2}{4r^2_{ys}} + \frac{z^2}{4r^2_{zs}}\Big) - f_l\Big(\frac{x^2}{4r^2_{xl}} + \frac{y^2}{4r^2_{yl}} + \frac{z^2}{4r^2_{zl}}\Big)\Big], \tag{6}$$

where λ, r_0, r_{xs}, r_{ys}, r_{zs}, r_{xl}, r_{yl}, r_{zl} are fit parameters and $f_s = 1/[1 + (r/r_0)^2]$, $f_l = 1 - f_s$. This 8-parameter Hump function achieves a better fit to the data ($\chi^2/\mathrm{ndf} = 1.4$). Smearing the track momenta by the measured resolution has a negligible effect on the data points and fits.

Figure 2(a)–2(c) shows a comparison of source function profiles in the x, y, and z directions [$S(r_x)$, $S(r_y)$, and $S(r_z)$] obtained via fitting (line) and source imaging (squares). Source image extraction makes no assumption for the shape of the 3D source function, whereas moment fitting explicitly assumes a shape. Therefore, the good agreement from the two extraction methods confirms the sufficiency of the Hump function but not its uniqueness.

The function $S(r_x)$ is characterized by a long tail, which is resolved up to ~60 fm, in contrast to $S(r_y)$ and $S(r_z)$ which range up to ~25 fm. This difference is also reflected

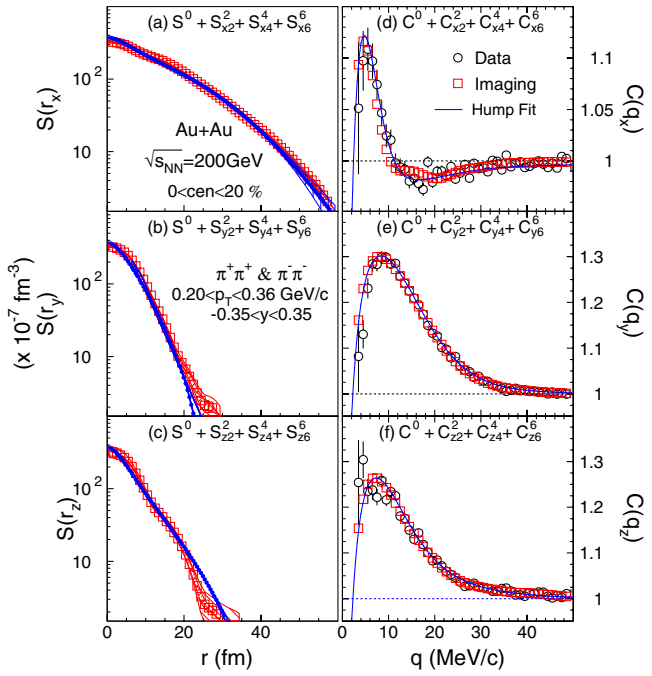

FIG. 2 (color online). Source function profiles $S(r_x)$, $S(r_y)$, and $S(r_z)$ (left panels) and their associated correlation profiles $C(q_x)$, $C(q_y)$, and $C(q_z)$ (right panels) in the PCMS. Symbols are as indicated. The bands indicate statistical and systematic errors.

in the respective correlation profiles [Figs. 2(d)–2(f)] obtained by summation of the data (circle), fit (line), and image (square) moments up to order $l = 6$ (Coulomb effects are not removed). The broader $S(r_x)$ is associated with the narrower $C(q_x)$ [Figs. 2(a) and 2(d)], as expected.

The extended tail lies along the pair total transverse momentum. Thus, the relative emission times between pions, as well as the source geometry, will contribute to $S(r_x)$. The source lifetime contributes to the range of $S(r_z)$, and $S(r_y)$ reflects its mean transverse geometric size. The difference between $S(r_x)$ and $S(r_y)$ is thus driven by the combination of the emission time difference, freeze-out dynamics, and kinematic Lorentz boost.

The event generator THERMINATOR [12,13] can shed more light on the source breakup and emission dynamics. It gives thermal emission from a longitudinally oriented cylinder of radius $\rho_{\max}$, includes all known resonance decays, and assumes Bjorken longitudinal boost invariance. The option for blast-wave transverse expansion was employed with radial velocity v_r semilinear in ρ [14], i.e., $v_r(\rho) = (\rho/\rho_{\max})/(\rho/\rho_{\max} + v_t)$, where $v_t = 1.41$. A differential fluid element is a ring defined by cylindrical coordinates z and ρ; it breaks up at proper time τ in its rest frame or at time t in the lab frame, where $t^2 = \tau^2 + z^2$. The freeze-out hypersurface is given by $\tau = \tau_0 + a\rho$, where τ_0 is the proper breakup time for $\rho = 0$ and a represents the slope of the freeze-out hypersurface in ρ-τ space (it sets the space-time correlation for particle emission: $a > 0$ implies earlier emission of particles at small ρ's, i.e., inside-out "burning" while $a < 0$ implies the reverse, i.e., outside-in "burning"). In blast-wave mode, THERMINATOR sets $a = -0.5$ for source emission from outside in as in many hydrodynamical models.

Using a set of parameters tuned to fit charged pion and kaon spectra [15], midrapidity pion pairs from THERMINATOR were obtained with the effects of all known resonance decay processes on and off. These pairs were then transformed to the PCMS, as in the data analysis, to obtain $S(r_i)$ distributions for comparison with the data.

Figure 3 shows that the 3D source function generated by THERMINATOR calculations (solid triangles) with $\tau_0 = 8.55$ fm/c, $\rho_{\max} = 8.92$ fm, and other previously tuned parameters [15], underestimates $S(r_x)$, $S(r_y)$, and $S(r_z)$. Open triangles (Fig. 3) show that resonance decays reproduce $S(r_y)$ [3(b)] and extend the calculated source function in x [3(a)] as expected, but not enough to account for the long tails in x and z (these are longer than THERMINATOR source profiles with resonance decays alone). This suggests that they have substantial contribution from pion pairs with significantly longer emission time differences. Attempts to fit the distributions by only increasing τ_0 or with $a \geq 0$ failed. The requirement of $a < 0$ in order to reproduce the extracted source function suggests a fireball burning from outside in.

The generated distribution of time differences can also be lengthened by sampling pions from a family of hyper-

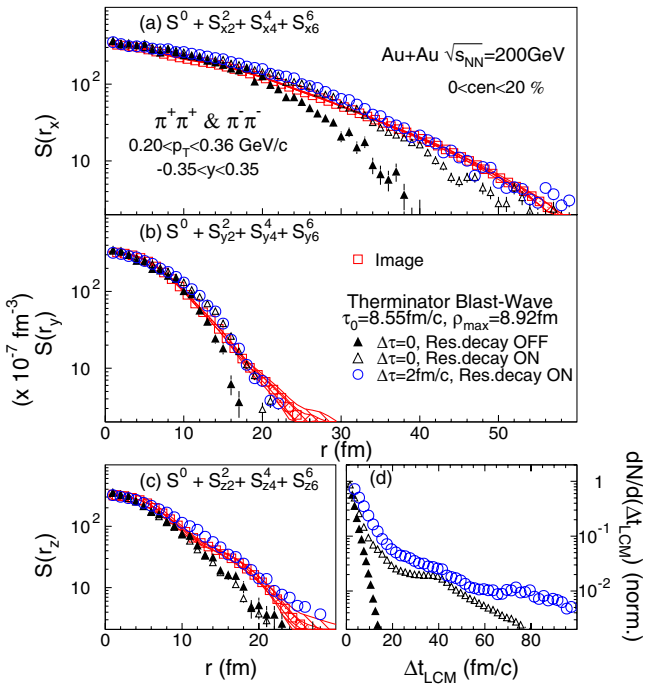

FIG. 3 (color online). Source function comparison between THERMINATOR calculation and image for (a) $S(r_x)$, (b) $S(r_y)$, (c) $S(r_z)$ in PCMS. Panel (d) compares Δt_{LCM} from THERMINATOR events with various assumptions for $\Delta\tau$ and resonance emission.

surfaces defined by a range of values of proper breakup times τ'. One such parametrization consists of replacing τ by τ' chosen from an exponential distribution $dN/d\tau' = \frac{\Theta(\tau'-\tau)}{\Delta\tau}\exp[-(\tau'-\tau)/\Delta\tau]$, where the width of the distribution $\Delta\tau$ represents the mean proper emission duration. Figure 3 shows that this approach, with $\Delta\tau = 2$ fm/c (open circles), leads to a fairly good match to the three observed source profiles. A 10% change in $\Delta\tau$ (with other parameters unchanged) spoils this match.

Figure 3(d) shows the relative emission time distribution in the LCMS, Δt_{LCM}, for pion pairs from events with the parametrizations indicated. For a fixed $\tau_0 = 8.55$ fm/c ($\Delta\tau = 0$) and resonance decays excluded, the distribution Δt_{LCM} is narrow, $\langle|\Delta t_{\mathrm{LCM}}|\rangle = 2.4$ fm/c. The addition of resonance decays adds a long tail and gives $\langle|\Delta t_{\mathrm{LCM}}|\rangle = 8.8$ fm/c. Replacing τ with the exponential distribution τ' with $\Delta\tau = 2$ fm/c results in a Δt_{LCM} distribution which is significantly broadened to give $\langle|\Delta t_{\mathrm{LCM}}|\rangle = 11.8$ fm/c. The wider distribution of time delays is needed to reproduce the source distributions. This implies a finite nonzero proper emission duration in the emission rest frame. Note that this Δt_{LCM} distribution broadening has only a small effect on $S(r_y)$.

The source distensions in Fig. 3 point to substantial time differences Δt_{LCM}; however, the interplay between proper time and breakup dynamics is model dependent. Nevertheless, the picture emerging from the data, in the context of the THERMINATOR model, is consistent with an expanding fireball of proper breakup time $\tau_0 \sim 9$ fm/c which hadronizes and emits particles over a short but nonzero mean proper emission duration $\Delta\tau \sim 2$ fm/c.

In summary, a new model-independent, three-dimensional source imaging technique has been applied to extract the 3D pion emission source function in the PCMS frame from Au + Au collisions at $\sqrt{s_{NN}} = 200$ GeV. The source function has a much greater extent in the out (x) and long (z) than in the side (y) direction. THERMINATOR model comparison indicates a fireball burning from outside in with proper lifetime $\tau_0 \sim 9$ fm/c and a mean proper emission duration $\Delta\tau \sim 2$ fm/c, leading to significant relative emission times ($\langle|\Delta t_{\mathrm{LCM}}|\rangle \approx 12$ fm/c), including those due to resonance decay.

We thank the staff of the Collider-Accelerator and Physics Departments at BNL for their vital contributions. We thank P. Danielewicz, A. Kisiel, and S. Pratt for their interest and input. We acknowledge support from the Office of Nuclear Physics in DOE Office of Science and NSF (U.S.), MEXT and JSPS (Japan), CNPq and FAPESP (Brazil), NSFC (China), IN2P3/CNRS and CEA (France), BMBF, DAAD, and AvH (Germany), OTKA (Hungary), DAE (India), ISF (Israel), KRF and KOSEF (Korea), MES, RAS, and FAAE (Russia), VR and KAW (Sweden), U.S. CRDF for the FSU, US-Hungarian NSF-OTKA-MTA, and US-Israel BSF.

*Deceased.
†PHENIX Spokesperson.
jacak@skipper.physics.sunysb.edu

[1] *Proceedings of Quark Matter 2006*, edited by Y.-G. Ma, E.-K. Wang, X. Cai, H.-Z. Huang, X.-N. Wang, and Z.-Y. Zhu [J. Phys. G: Nucl. Part. Phys. 34, No. 8 (2007)].
[2] S. Pratt, Phys. Rev. Lett. **53**, 1219 (1984).
[3] S. E. Koonin, Phys. Lett. B **70**, 43 (1977).
[4] M. Lisa *et al.*, Annu. Rev. Nucl. Part. Sci. **55**, 357 (2005).
[5] D. A. Brown and P. Danielewicz, Phys. Lett. B **398**, 252 (1997); Phys. Rev. C **57**, 2474 (1998); **64**, 014902 (2001).
[6] P. Chung *et al.*, Nucl. Phys. **A749**, 275c (2005).
[7] S. S. Adler *et al.*, Phys. Rev. Lett. **98**, 132301 (2007).
[8] P. Danielewicz and S. Pratt, Phys. Lett. B **618**, 60 (2005).
[9] P. Danielewicz and S. Pratt, Phys. Rev. C **75**, 034907 (2007).
[10] K. Adcox *et al.*, Nucl. Instrum. Methods Phys. Res., Sect. A **499**, 469 (2003).
[11] R. Lednicky *et al.*, Phys. Part. Nucl. **35**, S50 (2004).
[12] P. Chung, J. Phys. G **35**, 044034 (2008)
[13] A. Kisiel *et al.*, Comput. Phys. Commun. **174**, 669 (2006).
[14] A. Kisiel, Braz. J. Phys. **37**, 917 (2007).
[15] A. Kisiel *et al.*, Phys. Rev. C **73**, 064902 (2006). Values used are $T = 165.6$ MeV for temperature, $\mu_B = 28.5$ MeV, $\mu_S = 6.9$ MeV, $\mu_I = -0.9$ MeV for baryon, strangeness, and isospin chemical potentials.